COMMUNICATION

Direct Evidence for Cation Non-Stoichiometry and Cottrell Atmospheres Around Dislocation Cores in Functional Oxide Interfaces

By *Miryam Arredondo, Quentin M. Ramasse, Matthew Weyland, Reza Mahjoub, Ionela Vrejoiu, Dietrich Hesse, Nigel D. Browning, Marin Alexe, Paul Munroe,* and *Valanoor Nagarajan**

Perovskite oxides are a ubiquitous class of functional oxide materials that are used in a variety of nanoscale functional applications.[1] In order to exploit their properties, these materials are often deposited on a dissimilar underlying substrate. A critical consequence of this process is the formation of misfit dislocation arrays at the film-substrate interface as a mechanism to release the lattice mismatch strain.[2] Although dislocation cores are only a few angstroms wide, the associated strain-fields are often significant and long-range. Theoretical computations of the strain-field for metals reveal that the stress due to the local strain around the core can be equal to or even higher, than the yield stress.[3]

Concurrently, the trend of aggressive downsizing has resulted in functional materials being confined to nanometric volumes. The presence of even a single defect, and its associated long-range field, could adversely affect device performance.[4,5] Such long-range strain fields are known to affect both the microstructure[6,7] and electronic states.[8,9] More recently the detrimental effect of this strain field on the polarization and electromechanical response of nanoscale ferroelectrics has been studied.[10–12] Conversely, defect-free ferroelectric thin films with perfectly coherent interfaces have been shown to possess very large ferroelectric polarization.[13] While the focus has been overtly on the physical aspect of the strain fields in ferroelectrics, information on the chemical implications of this strain field is relatively scarce. Investigations in $SrTiO_3$ (STO) show that dislocation cores are regions where chemistry is distinct from the bulk[4,14,15] and possess reversible switching of electrical properties.[16] However, STO is paraelectric at room temperature and does not possess remnant polarization. Therefore, the vital question of how variations in nanoscale local chemistry of a dislocation core impacts a ferroelectric interface still remains unanswered. This is critical, as non-stoichiometric cores can be charged and hence create enormous depolarization fields and/or pinned domain walls.[17] These have serious consequences on the operating voltages and scalability of electronic devices.

Here, we present a detailed atomic-scale study on the structural and chemical changes produced by edge dislocations at the growth interface between a perovskite oxide bottom electrode, $SrRuO_3$ (SRO), and the $PbZr_{0.52}Ti_{0.48}O_3$ (PZT) ferroelectric film (here onwards referred to simply as the *interface*). State-of-the-art spherical aberration-corrected scanning transmission electron microscopy (C_s-corrected STEM) imaging and spectroscopy techniques yield direct visual evidence for cation (Pb) excess and oxygen deficiency at the dislocation core.

Figure 1a is a Z-contrast image, acquired along [001] zone-axis for the (001) PZT-SRO interface. Three edge dislocations are clearly seen (enclosed in white boxes), located within the SRO layer just below the PZT-SRO interface (more dislocation images shown in S2a). The dislocations have a Burgers vector, $b = a\langle 010\rangle$ and the extra half-plane is located in the SRO layer, in agreement with previous HRTEM results.[11] Furthermore, a contrast variation around the dislocation core into the SRO layer is observed in Figure 1a. Typically, for dislocations such changes in contrast in Z-contrast imaging are attributed to very large strain levels present in regions in close proximity to the dislocation core.[18] Energy dispersive X-Ray (EDX) mapping was performed as a first approach to study the chemical origin of the observed contrast variation. Figure 1b shows a Z-contrast image, from a 10 nm × 10 nm area containing a single dislocation at the PZT-SRO interface. Figure 1c–1g show the raw EDX elemental maps, with a step size of 0.5 nm, for Pb, Ti, Sr, Zr and Ru respectively and Figure 1h is the corresponding Z-contrast image

[*] Dr. V. Nagarajan, M. A. Arredondo, R. Mahjoub, Prof. P. Munroe
School of Materials Science & Engineering
University of New South Wales
Sydney NSW 2052 (Australia)
E-mail: nagarajan@unsw.edu.au
Dr. Q. M. Ramasse
Lawrence Berkeley National Laboratory
Natl Ctr Electron Microscopy
1 Cyclotron Rd, Berkeley CA 94708 (USA)
Dr. M. Weyland
Monash Centre for Electron Microscopy
Monash University
Victoria 3800 (Australia)
Dr. I. Vrejoiu, Dr. M. Alexe, Prof. D. Hesse
Max Planck Institute of Microstructure Physics
Weinberg 2, 06120 Halle (Germany)
Prof. N.D. Browning
Department of Chemical Engineering and Materials Science,
Department of Molecular and Cellular Biology,
University of California
One Shields Ave, Davis CA 95616 (USA)
Prof. N.D. Browning
Physical and Life Sciences Directorate
Lawrence Livermore National Laboratory
Livermore CA 94550 (USA)

DOI: 10.1002/adma.200903631

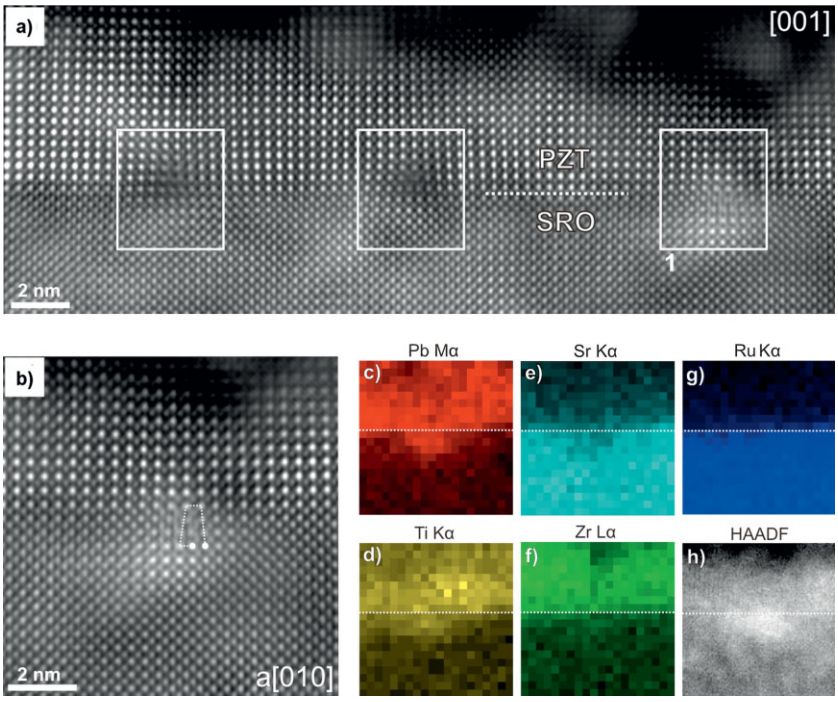

Figure 1. Z-contrast image and EDX mapping of the [001] PZT-SRO interface. a) Z-contrast image showing three edge dislocations at the interface, enclosed in the white boxes. b) Digitally magnified Z-contrast image from the box marked as 1 in Figure 1a, showing an a[010] edge dislocation and its Burgers vector. Elemental maps for: c) Pb Mα, d) Ti Kα, e) Sr Kα, f) Zr Lα, and g) Ru Kα. h) Z-contrast image used as a reference for the elemental maps, the white and black dotted lines mark the interface.

used as reference for the elemental maps. Z-contrast images were acquired before and after the EDX analysis, confirming that no beam damage occurred (S2). In Figure 1c one notices clear diffusion of Pb across the PZT-SRO interface (marked by a white dotted line) with a slightly asymmetric "U" shaped cup indicating radial distribution of Pb around the dislocation line in the SRO layer. Within the spatial resolution of each pixel, the area covered by this cup is in close agreement to the bright regions around the dislocation in Figure 1b and 1h. Thus, we ascertain that the contrast variation around the dislocation core is a result of Pb segregation around the core (although an additional contribution from strain contrast cannot be excluded). The EDX map for Ti and Zr (Figure 1d, 1f) also indicates Ti and Zr diffusion into the SRO layer, although this is not as clearly evident as in the case for Pb. Conversely, Sr (Figure 1e) shows deficiency at the same region. When comparing Figure 1c and 1e, the Pb diffusion presents a cup shape that correlates with the Sr elemental map, indicating commensurate Sr deficiency. The EDX maps presented here provide evidence for Pb segregation around the dislocation core. Finally, we show that Ru (Figure 1g) exhibits no diffusion (also previously confirmed[19]) and hence, it was used to locate the interface.

The EDX mapping above was complemented by atomic-scale EELS analysis to further explore the effect of the cation variations on the electronic configurations of the oxygen sublattice at and around the dislocation core. Recent developments in atomically-resolved, column-by-column EEL spectra acquisition,[20–22] provide spectrum imaging or line scan techniques with unprecedented energy and spatial resolution.[23–27] Figure 2a shows a Z-contrast image of a single dislocation at the PZT-SRO interface, indicating the probe positions used to acquire the EEL spectra shown in Figure 2b. Acquired along the direction of the extra atomic plane through the dislocation core, it starts from the PZT layer (position 1) and proceeds down to the SRO (position 6). Positions 4 and 5 show the data for the limit of the strained region, simply referred to as border of the dislocation. For purposes of statistical confidence, several such series were collected which yielded identical information (S3). All EEL spectra were treated with principal component analysis (PCA).[28] Although the overlap of the Ti–$L_{2,3}$ and Ru–M_3 edges in the 440 to 460 eV region prevents any quantitative analysis to be obtained, these edges do provide a qualitative understanding. The sharp and well-defined "white lines" (peaks labeled *a* and *b* on Figure 2b) of the Ti–$L_{2,3}$ edge become shorter and broader as the probe is moved from position 1 to 6. The pronounced shoulder on the left of peak *a*, an edge onset shifting to a slightly lower energy, is attributed to the increased contribution of the Ru-M_3 edge (~445 eV).[29] Whilst there is a noticeable intensity decrease in the Ti signal, both *a* and *b* peaks remain present within the SRO and at the dislocation core, while

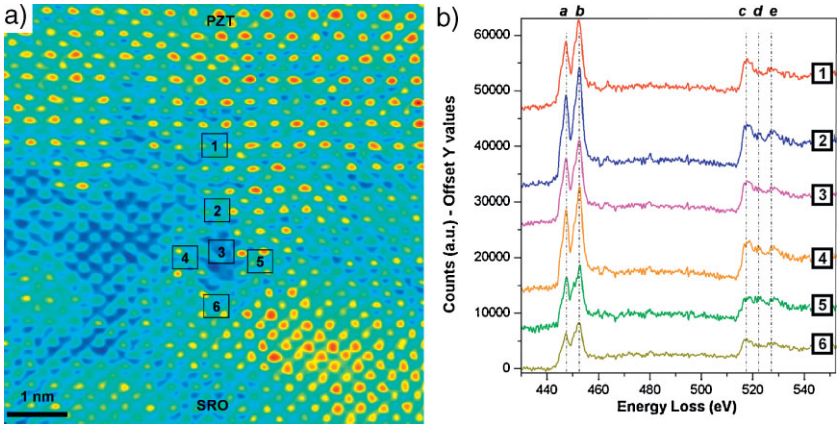

Figure 2. EELS profiles for Ti-$L_{2,3}$, Ru-M_3 and O–K edges. a) Guide for the EELS positions: deconvoluted Z-contrast image of the [001] PZT-SRO interface, the intensity is displayed on a false color scale to improve visibility. b) EEL spectra for Ti-$L_{2,3}$ and Ru-M_3 edges: the EELS profiles were recorded from the PZT layer (position 1), dislocation core (position 3), borders (position 2, 5, 4) and the SRO layer (position 6). *a* and *b* represent the Ti-$L_{2,3}$ and Ru-M_3 edges, while *c*–*e* represent the three major peaks for the O–K edge.

mainly a broad Ru-M_3 peak appears in spectra acquired in the bulk of the SRO film (S3). Furthermore, the broadening of the L_3 and L_2 white lines is consistent with a decrease in splitting of the e_g and t_{2g} sub-peaks due to a decrease of crystal-field splitting. This results in less-defined electronic states and, thus, broader and shorter peaks, as observed most clearly at positions 5 and 6. Similar effects have been reported in closely related cases for defects in STO, where they were attributed to the under-coordination of the Ti atoms as well as a change in Ti−O bond length.[30] The 510–540 eV region of the EEL spectra in Figure 2b shows three major peaks (labeled *c* to *e*). From prior reports, it is possible to assign the presence of peaks *c* and *d* to the interaction of O 2*p* states with Ti or Ru 3*d* bands,[14,31,32] while peak *e* maps bands with counter-ion character[31] such as Ti 4*sp*, Pb 6*s* and 6*p* bands. Here, the relative intensity of peak *c* correlates to the strength of the Ti or Ru signal. For example, positions 1, 2 and 4 (in contrast to position 5), show strong Ti $L_{2,3}$ white lines and exhibit a correspondingly strong peak *c* in the O–K edge. The most striking feature of the O-K edges, however, is the common characteristic of a strong peak *d* in spectra taken at or near the core of the dislocation at positions 2, 3, 5 and 4. It was suggested that the intensity ratio of peaks *c* and *d* reflects the linearity of the Ti−O−Ti bonds between the O atom and its two nearest Ti neighbors.[14] A large ratio, as is the case in bulk STO or here in position 6 or 1 is typical of an unperturbed linearity. Conversely, previous studies on STO have attributed a smaller ratio to oxygen deficiency at the core of dislocations or grain boundaries,[14,15,30,33] and furthermore incomplete oxygen octahedra at such defect sites.[34] Our results thus, suggest that the fine structure changes observed in the O–K edge at the dislocation core are the signature of oxygen deficiency. This is not unexpected; for excess Pb atoms to be accommodated in the SRO lattice, they would have to be closer to each other in the extra-half planes due to their larger ionic radii (discussed later). This would be most easily possible for the dislocation core by creating oxygen vacancies. Additionally, the analysis of the O–K edge EEL spectra strongly suggests a higher Ti/O ratio in the core, which is consistent with the oxygen vacancies requirement and, thus, ensuing non-stochiometry in the dislocation core.

Multi-slice image simulations were carried out to confirm the atomic arrangements inferred from the spectroscopic measurements. It should be noted at this point that some structural variations along the beam direction could be expected: depending on sample thickness, the dislocation core may not run all the way form the top to the bottom surfaces of the specimen for instance, thus affecting the results. However, thanks to the reduced depth of field provided by aberration-corrected STEMs it is now possible to detect defects buried within samples by varying the defocus at which HAADF images are acquired.[35,36] Care was taken here to analyze only dislocations where no such structural variation was observed: through-focus series in other areas (not shown here) did indeed reveal the presence of buried cores that did not reach the surface. It is therefore justified to assume that within the limited depth precision of this sectioning technique (about 3 nm for our settings) and for the specific areas analyzed in this study, no structure changes were present through the sample thickness. Based on the above experimental results, two structures for the Pb-rich dislocation core were proposed: symmetric and asymmetric (S4). To yield a fully quantitative comparison between simulated and experimental images, care was taken to characterize precisely all experimental parameters (sample thickness, detector response, effective probe size, optical aberration coefficients, etc.). Thus both can be displayed clearly with the same intensity color scale.[37] The experimental images were deconvoluted to remove noise using a maximum entropy algorithm,[38] although raw data are also presented here: Figure 3a (3b) and 3c (3d) show the raw and deconvoluted data for the symmetric (asymmetric) structure, respectively. Figure 3e

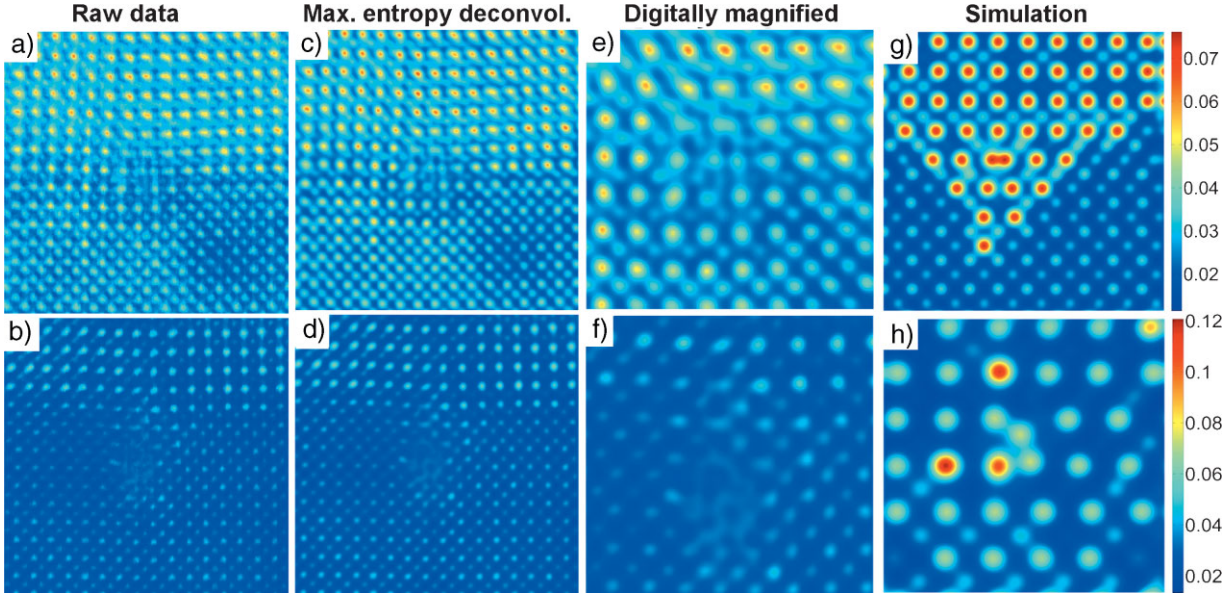

Figure 3. Simulation datasets for asymmetric and symmetric edge dislocations. Data set for the symmetric (asymmetric) dislocation: a) (b) experimental raw data, c) (d) image after using maximum entropy deconvolution, e) (f) digitally magnified image (after being deconvoluted) and g) (h) multislice simulation.

(3f) is a digitally magnified image of Figure 3c (3d) and Figure 3g (3h) corresponds to the simulation. The contrast arising from the presence of the extra Pb atom in the model is well matched in the simulation and the observed atomic arrangement is reproduced reasonably well for the symmetric dislocation core (Figure 3a, 3c, 3e, and 3g). Although the contrast levels for the asymmetric structure (Figure 3b, 3d, 3f, and 3h) are not as closely matched (most likely due to the small cell size, S4), the overall structure is still remarkably well reproduced. These results provide the first direct proof of Pb non-stoichiometry and thus charged dislocation cores in ferroelectric interfaces. Given the prior understanding of the strong link between charged cores and depolarization fields,[10] we are thus able to supply reasons why ferroelectricity in the vicinity of a dislocation core is found to be drastically compromised.

Figure 3 shows that the excess Pb atoms are spatially found ~1 nm from the dislocation core. These regions very close to the core are typically highly influenced by the strain field of the dislocation. Hence we investigated stress-assisted diffusion,[39–41] to explain the distribution of excess atoms around the dislocation (the so-called Cottrell atmosphere).[40,42]

Geometric phase analysis (GPA) was performed to quantify the strain around the dislocation core relative to the SRO layer (Figure 4a–c). The GPA reveals no contrast in the ε_{xy} shear, but ε_{yy} shows very large dilation (~14%) in the PZT layer in close proximity to the core. Thus we confirm enormous strain levels at the proximity of the core (full discussion found in S5). The stress-assisted segregation of a cation onto edge dislocations can then be analyzed by using the modified Cottrell and Bilby formulation[42,43] (derived in S6). In Figure 4d, we link results of this model, to the two-dimensional strain maps around the dislocation, obtained by GPA for the experimental datasets. It plots the so-called excess solute flux Q due to the stress-assisted diffusion coefficient and shows that the excess flux rapidly approaches zero for distances beyond 1 nm from a dislocation core, in agreement with the experiment.

In conclusion, we have used C_s-corrected STEM and atomic-scale spectroscopy techniques to investigate the chemical consequences of the long-range strain fields associated with dislocation cores at a functional oxide interface. The STEM observations are supported by quantitative models that predict stress-assisted segregation of Pb around the dislocation cores. Considering the general sensitivity of the functional properties of perovskites against variations of the chemical composition, it can be assumed that the new findings will have a considerable impact on the microstructure-property relations of nanoscale functional devices.

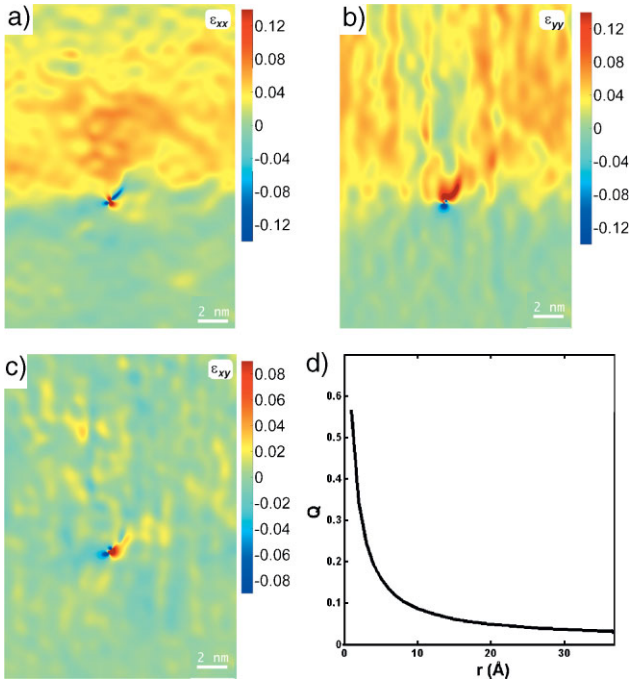

Figure 4. Two-dimensional strain maps obtained by GPA and precipitation onto an edge dislocation. a) ε_{xx}, b) ε_{yy}, and c) ε_{xy} are the strain tensor components for the symmetric dislocation in Figure 3a. Note that tensor components are expressed as a percentage relative to the SRO lattice and displayed with an intensity color scale d) Stress-assisted precipitation onto an edge dislocation, calculated from Cottrell–Bilby equation. The flux (Q) rapidly approaches zero for distances beyond 10 Å (r) from the dislocation core.

Experimental

Specimens for high resolution STEM investigations were prepared by standard procedures [44] from a $PbZr_{0.52}Ti_{0.48}O_3$ (PZT)/$SrRuO_3$ (SRO)/$SrTiO_3$ (STO) heterostructure, grown by pulsed laser deposition [13]. Z-contrast imaging and EDX analysis were performed using a double-corrected FEI Titan^3 80-300 microscope, equipped with an EDAX detector and operated at 300 kV and 80 kV, respectively. Point-by-point EELS analysis was performed over 10 equivalent regions containing dislocations in a dedicated STEM (Nion-corrected VG HB 501) operated at 100kV and equipped with an Enfina parallel EELS detector. To confirm that no beam damage occurred, images before and immediately after the EELS acquisition were obtained (S2). Detailed Z-contrast imaging, EELS acquisition and simulations parameters can be found in the supplementary sections.

Acknowledgements

The authors would like to thank CONACYT Mexico, ARC DP 0666231, Office of Science, Office of Basic Energy Sciences of the US Department of Energy through grant number DE-FG02-03ER46057 and DE-AC02-05CH11231, the German Science Foundation (DFG) via SFB 762 and DEST International Linkage Grant for their support on this project. Supporting Information is available online from Wiley InterScience or from the author.

Received: October 23, 2009
Published online: April 29, 2010

[1] R. Waser, *Nanoelectronics and Information Technology: Advanced Electronic Materials and Novel Devices*, Wiley-VCH, Germany **2005**.
[2] J. W. Matthews, *Philo. Mag.* **1974**, *29*, 797.
[3] F. R. N. Nabarro, *Dislocations in Solids*, North-Holland Pub. Co New York **1979**.
[4] M. F. Chisholm, S. J. Pennycook, *Philo. Mag.* **2006**, *86*, 4699.
[5] M. J. Hÿtch, J.-L. Putaux, J.-M. Pénisson, *Nature* **2003**, *423*, 270.
[6] S. Y. Hu, Y. L. Li, L. Q. Chen, *J. Appl. Phys.* **2003**, *94*, 2542.

[7] S. K. S. S. Stemmer, F. Ernst, M. Ruehle, W.-Y. Hsu, R. Raj, *Solid state ionics* **1995**, *75*, 43.
[8] I. Arslan, A. Bleloch, E. A. Stach, N. D. Browning, *Phys. Rev. Lett.* **2005**, *94*, 5504.
[9] L. Lymperakis, J. Neugebauer, M. Albrecht, T. Remmele, H. P. Strunk, *Phys. Rev. Letts.* **2004**, *93*, 169401.
[10] C. L. Jia, S. B. Mi, K. Urban, I. Vrejoiu, M. Alexe, D. Hesse, *Phys. Rev. Lett.* **2009**, *102*, 117601.
[11] M. W. Chu, I. Szafraniak, R. Scholz, C. Harnagea, D. Hesse, M. Alexe, U. Gösele, *Nat. Mater.* **2004**, *3*, 87.
[12] V. Nagarajan, C. L. Jia, H. Kohlstedt, R. Waser, I. B. Misirlioglu, S. P. Alpay, R. Ramesh, *Appl. Phys. Lett.* **2005**, *86*, 192910.
[13] I. Vrejoiu, G. Le Rhun, L. Pintilie, D. Hesse, M. Alexe, U. Göesele, *Adv. Mater.* **2006**, *18*, 1657.
[14] Z. L. Zhang, W. Sigle, M. Ruehle, *Phys. Rev. B* **2002**, *66*, 4108.
[15] C. L. Jia, A. Thust, K. Urban, *Phys. Rev. Lett.* **2005**, *95*.
[16] K. Szot, W. Speier, G. Bihlmayer, R. Waser, *Nat. Mater.* **2006**, *5*, 312.
[17] A. Y. Emelyanov, N. A. Pertsev, *Phys. Rev. B* **2003**, *68*, 214103.
[18] I. Arslan, N. D. Browning, *Microscopy Research and Technique* **2006**, *69*, 330.
[19] M. Arredondo, M. Saunders, A. Petraru, H. Kohlstedt, I. Vrejoiu, M. Alexe, D. Hesse, N. D. Browning, P. Munroe, V. Nagarajan, *J. Mater. Sci.* **2009**, *44*, 5297.
[20] L. J. Allen, S. D. Findlay, A. R. Lupini, M. P. Oxley, S. J. Pennycook, *Phys. Rev. Lett.* **2003**, *91*, 4.
[21] M. Bosman, V. J. Keast, J. L. Garcia-Munoz, A. J. D'Alfonso, S. D. Findlay, L. J. Allen, *Phys. Rev. Lett.* **2007**, 99.
[22] L. Fitting Kourkoutis, S. Thiel, A. Schmehl, J. Mannhart, D. A. Muller, *Ultramicroscopy.* **2006**, *106*, 1053.
[23] M. Varela, T. J. Pennycook, W. Tian, D. Mandrus, S. J. Pennycook, V. Pena, Z. Sefrioui, J. Santamaria, "Atomic scale characterization of complex oxide interfaces", presented at *10th Meeting on Frontiers of Electron Microscopy in Materials Science*, Maastricht, The Netherlands, September **2005**.
[24] J. C. Loudon, L. Fitting Kourkoutis, J. S. Ahn, C. L. Zhang, S. W. Cheong, D. A. Muller, *Phys. Rev. Lett.* **2007**, *99*.
[25] G. Yang, Q. Ramasse, R. F. Klie, *Phys. Rev. B* **2008**, *78*.
[26] D. A. Muller, L. F. Kourkoutis, M. Murfitt, J. H. Song, H. Y. Hwang, J. Silcox, N. Dellby, O. L. Krivanek, *Science* **2008**, *319*, 1073.
[27] D. A. Muller, N. Nakagawa, A. Ohtomo, J. L. Grazul, H. Y. Hwang, *Nature* **2004**, *430*, 657.
[28] M. Watanabe, M. Kanno, D. Ackland, C. Kiely, D. Williams, *Microscopy and Microanalysis* **2007**, *13*, 1264.
[29] C. C. Ahn, O. L. Krivanek, R. P. Burger, A. S. University, M. M. Disko, EELS Atlas: A Reference Collection of Electron Energy Loss Spectra Covering All Stable Elements, HREM Facility, Center for Solid State Science, Arizona State University; Gatan, Inc, **1983**.
[30] J. P. Buban, M. F. Chi, D. J. Masiel, J. P. Bradley, B. Jiang, H. Stahlberg, N. D. Browning, *J. Mater. Res.* **2009**, *24*, 2191.
[31] L. F. Fu, S. J. Welz, N. D. Browning, M. Kurasawa, P. C. McIntyre, *Appl. Phys. Lett.* **2005**, *87*.
[32] A. D. Lozano-Gorrin, J. E. Greedan, P. Nunez, C. Gonalez-Silgo, G. A. Botton, G. Radtke, *J. Solid State Chem.* **2007**, *180*, 1209.
[33] M. Kim, G. Duscher, N. D. Browning, K. Sohlberg, S. T. Pantelides, S. J. Pennycook, *Phys. Rev. Lett.* **2001**, *86*, 4056.
[34] N. D. Browning, J. P. Buban, H. O. Moltaji, S. J. Pennycook, G. Duscher, K. D. Johnson, R. P. Rodrigues, V. P. Dravid, *Appl. Phys. Lett.* **1999**, *74*, 2638.
[35] K. van Benthem, A. R. Lupini, M. P. Oxley, S. D. Findlay, L. J. Allen, S. J. Pennycook, *Ultramicroscopy* **2006**, *106*, 1062.
[36] C. Kisielowski, B. Freitag, M. Bischoff, H. van Lin, S. Lazar, G. Knippels, P. Tiemeijer, M. van der Stam, S. von Harrach, M. Stekelenburg, M. Haider, S. Uhlemann, H. Muller, P. Hartel, B. Kabius, D. Miller, I. Petrov, E. A. Olson, T. Donchev, E. A. Kenik, A. R. Lupini, J. Bentley, S. J. Pennycook, I. M. Anderson, A. M. Minor, A. K. Schmid, T. Duden, V. Radmilovic, Q. M. Ramasse, M. Watanabe, R. Erni, E. A. Stach, P. Denes, U. Dahmen, *Microscopy and Microanalysis* **2008**, *14*, 469.
[37] J. M. LeBeau, S. D. Findlay, L. J. Allen, S. Stemmer, *Phys. Rev. Lett.* **2008**, *100*.
[38] K. Ishizuka, E. Abe, Proc. of the 13th European Microscopy Congress (13th EMC) Instrumentation and Methodology **2004**, 1, p. 117.
[39] J. Hirth, J. Lothe, *Theory of Dislocations*, McGraw-Hill, New York **1968**.
[40] H. Mehrer, Diffusion in Solids, Vol.155, Springer Series in Solid-State Sciences, **2007**.
[41] P. G. Shewmon, *Diffusion in Solids*, McGraw-Hill, New York **1989**.
[42] L. V. Meisel, *J. Appl. Phys.* **1967**, *38*, 4780.
[43] A. H. Cottrell, B. A. Bilby, *Proc. Phys. Soc. London Section A* **1949**, *62*, 49.
[44] D. B. Williams, C. B. Carter, *Transmission Electron Microscopy*, Plenum Press, New York **1996**.